Chem Rev Lett 6 (2023) 223-234

Research Article

Chemical Review and Letters
journal homepage: www.chemrevlett.com
ISSN (online): 2645-4947 (print) 2676-7279

Investigation of Ti—B nanoheterofullerenes evolved from C20 nanocage through DFT

Maryam Koohi[1], Hajieh Bastami[2, *]

[1]*Department of chemistry, Technical and Vocational University (TVU), Tehran, Iran*
[2]*Department of materials and Metallurgical Engineering, Technical and Vocational University (TVU), Tehran, Iran*

ARTICLE INFO

Article history:
Received 21 March 2023
Received in revised form 17 July 2023
Accepted 17 July 2023
Available online 10 August, 2023

Keywords:
$C_{20-2n}Ti_nB_n$
Heterofullerene
Substituent effect
Stability

ABSTRACT

In present computational survey, we are compared and contrasted electronic effects of C_{20} and its $C_{20-2n}Ti_nB_n$ heterofullerenic derivatives with n = 1-5, at density functional theory (DFT). All nanocages are true minima and none of them collapses to deformed open cage as segregated nanostructure. Isolating five single hetero bonds of Ti—B *via* either one double bond of C═C or one carbon atom is a suitable method for reaching highly substituted stable heterofullerene *i.e.* pen-shell $C_{10}Ti_5B_5$ since it prevents from weak homo bonding of Ti—Ti and B—B. The C_1-$C_{18}Ti_1B_1$ heterofullerene can avoid from the most strained directly fused five-pentagon configuration, but its open-shell electronic structure with highly pyramidalized titanium atom (126.59° *i.e.* 3-4 times relation to C_{20}) may render it too reactive to be observed under typical experimental conditions. The calculated binding energy (*B.E.*) shows $C_{10}Ti_5B_5$ as the most stable heterofullerene. Contrary on *B.E.*, the absolute heat of atomization of heterofullerenes decreases as number of substituting Ti—B unit (n) increases. Hence, substitution effect on binding energy is more significant than heat of atomization. Compared to the previously reported material such Ti-decorated B_{38} nanofullerene as a suitable hydrogen storage with *B.E.* of 5.67 eV/atom, our studied $C_{20-2n}Ti_nB_n$ heterofullerenes show the higher *B.E.* with range of 12.25 to 38.03 eV/atom, the higher stability and the higher capacity for hydrogen storage. Interestingly, $C_{18}Ti_1B_1$ heterofullerene must be not only kinetically stable against electronic excitations but also based on natural bond orbital (NBO) analysis, the highest charge transfer (CT) is take placed from $\pi_{C=C}$ bonds to the neighboring LP^*_B, LP^*_{Ti} and σ^*_{Ti-B} anti-bonds of it. Also, the exceptionally large value of nucleus-independent chemical shifts (NICS) is found for $C_{18}Ti_1B_1$ compared to the archetypically aromatic benzene and [2.2]paracyclophane molecules.

1. Introduction

Substituting for carbon atoms in nanostructures with different heteroatoms has been the object of a wealth of experimental and computational studies aimed at unraveling their geometrical and electronic properties for example polymorphism, extraordinary hardness, band gap, chemical reactivity, *etc*. [1]. The special properties of nanostructured synthetic carbon allotropes can be related to the curved π-conjugation within their curved hexagonal, pentagonal and hybrid hexagon-pentagon carbon-carbon networks [2]. The curvature leads to a loss of spatial overlap of the atomic p orbitals and a shift in hybridization of the carbon atoms from the sp^2 of graphite to a state intermediate between sp^2 and sp^3 [3].

Boron-substituted fullerene is appropriate as a substrate since it consists of light elements and has the capability to bind with metal atoms such as Ti, Zr and U [4,5]. After B_{80} fullerene [6], different types of B-doped

* Corresponding author.; e-mail: mkouhi110@gmail.com
https://doi.org/10.22034/crl.2023.392356.1222

fullerenes (from B_{32} to B_{80}) have been suggested [4-8]. The alkali and alkaline-earth decorated boron fullerenes (B_{38} and B_{80}) have been commonly suggested as candidates for hydrogen storage [4-8]. The Ti-decorated fullerenes (B_{38}, B_{40} and $C_{24}B_{24}$) along with other nanostructures (Ti-coated graphene nanoribbons) also have been widely suggested as potential hydrogen storage materials [4-8]. All of the research mentioned above encourages us to examine whether the transition metal Ti atom decorated B_{38} fullerene is an efficient hydrogen storage media. There is little research on hydrogen storage and other properties of nanostructures of the form $C_{20-2n}Ti_nB_n$ [9-13]. Since the bulk boron cannot be found in nature, the design and synthesis of bulk boron allotropes and boron-substituted fullerenes still keeps challenging to theoretical and experimental chemists. Boron fullerenes are seen as efficient hydrogen storage media since they are light-weight and have the capability to bind with metaled atoms. Since isolated transition metal has the ability to bind a certain number of hydrogens, theoretical simulations on hydrogen adsorption by Ti—B heterofullerenes are reported as organotitanium compounds that we hope provide useful information. Thus, the aim of this paper is to survey hydrogen storage capacity of $C_{20-2n}Ti_nB_n$ heterofullerenes (n = 1-5) by DFT (Figure 1)

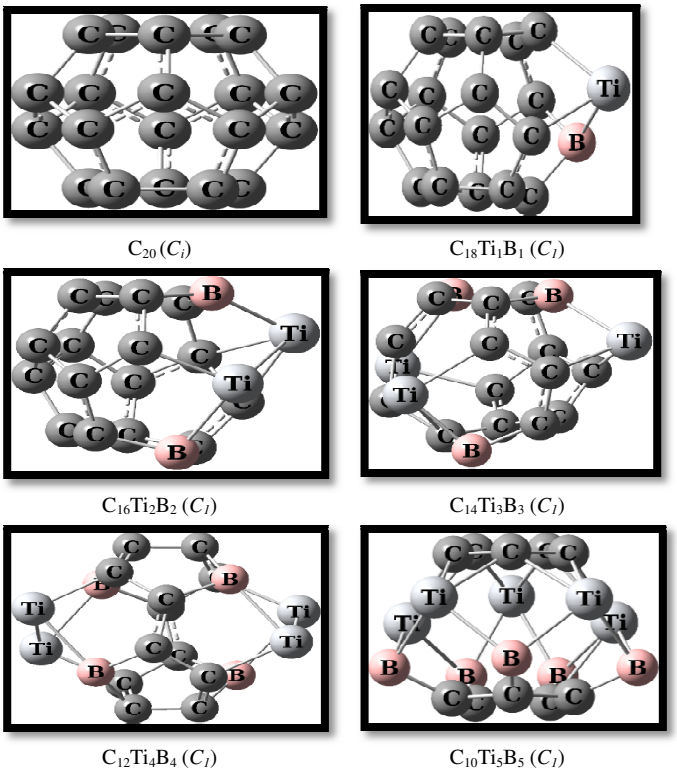

Fig. 1. Full optimized structures of C_{20} and $C_{20-2n}Ti_nB_n$ heterofullerenes (n = 1-5) along with their corresponding symmetries, at B3LYP/AUG-cc-pVTZ.

The Ti atoms can be substituted to carbon atoms of the $C_{20-n}B_n$ heterofullerenes (n = 1-5) due to the CT from the Ti atom(s) to boron and carbon atoms. Our results indicate that a strong binding among Ti atoms and the substituted boron of heterofullerenes can be efficiently prevents from segregation of $C_{20-2n}Ti_nB_n$ nanocages.

2. Computational Methods

In this survey, full geometry optimization and harmonic frequency calculations of C_{20} and $C_{20-2n}Ti_nB_n$ heterofullerenes are carried out without any symmetry constraints using hybrid functional B3LYP/6-311+G* [14] and the GAMESS program [15]. To reach more accurate energetic data, single point calculations for closed-shell multiplicity (n = 0, 2 and 4) are accomplished at restricted spin□symmetry methods of B3LYP/6-311++G**, M06-2X/6-311++G** [16] and B3LYP/AUG-cc-pVTZ based on the B3LYP/6-311+G* and M06-2X/6-311+G* geometries, respectively [17]. Structures with open-shell multiplicity (n = 1, 3 and 5) are optimized using unrestricted spin□symmetry methods including UB3LYP/6-311++G**, UM06-2X/6-311++G** and UB3LYP/AUG-cc-pVTZ based on UB3LYP/6-311+G* and UM06-2X/6-311+G* geometries, respectively. As a thermodynamic stability criterion of nanocages, binding energies are calculated according to the following expression: $B.E. = [(20-2n)E_C + nE_{Ti} + nE_B - E_{tot}] / 20$ where E_C, E_{Ti}, E_B, E_{tot} is the energy of carbon, titanium, boron atoms and total energy of the fullerene, respectively. The E_C, E_{Ti} and E_B values are guessed to be -37.86, -844.42 and -24.66 hartree, respectively, at the B3LYP/6-311+G*. As a kinetic stability criterion of nanocages, the NBO analysis on optimized structures is achieved, at B3LYP/AUG-cc-pVTZ, M06-2X/6-311++G** and B3PW91/6-311++G** [18, 19]. The NICS parameter is calculated at the centers of nanocages [20]. In addition, heat of atomization (ΔH_{at}) is accessible *via* the following expression: ΔH_{at} ($C_{20-2n}Ti_nB_n$) = ΔH_f ($C_{20-2n}Ti_nB_n$) – (20-2n)ΔH_f (C) – nΔH_f (Ti) – nΔH_f (B) where ΔH_f symbolizes the heat of formation. Then ΔH_f ($C_{20-2n}Ti_nB_n$) = E_{tot} - (20-2n)E_C – nE_{Ti} – nE_B, where E_{tot}, E_C, E_{Ti} and E_B, is total energy of heterofullerene, energy of carbon, titanium and boron atoms, respectively. The experimental values for H_f (C), H_f (Ti) and H_f (B), are 171.37, 111.85 and 77.92 kcal/mol, respectively [21]. The nucleophilicity index, N, is calculated as $N = E_{HOMO(Nu)} - E_{HOMO(TCNE)}$; (tetracyanoethylene (TCNE) is preferred as the reference) [22]. The global electrophilicity, ω is calculated *via* the following expression, $\omega = (\mu^2 / 2\eta)$, where μ is the chemical

potential ($\mu = (E_{HOMO} + E_{LUMO}) / 2$) and η is the global hardness ($\eta = (E_{LUMO} - E_{HOMO}) / 2$) [22].

3. Results and discussion

Before the optimization of the scrutinized structures such as $Ti_6B_6C_8$ and $Ti_7B_7C_6$ we completed conformer distribution analysis by Spartan 10 program and attained their relative energies along with their stabilities. Then, full optimization done without any symmetry constraints using the same methods and basis sets under study in this work (Figure 2).

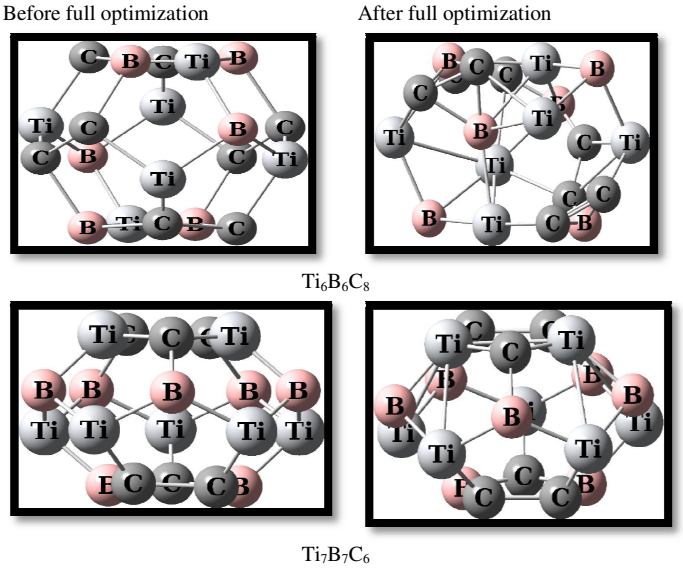

Fig. 2. Full optimized structures of $Ti_6B_6C_8$ and $Ti_7B_7C_6$ heterofullerenes, at B3LYP/AUG-cc-pVTZ.

Apparently, the fullerenic structures of $Ti_6B_6C_8$ and $Ti_7B_7C_6$ lose their uniformity due to the higher covalent radii of titanium (1.40 Å) compared to carbon (0.70 Å) and boron (0.85 Å) also shorting of Ti—Ti distances in equatorial and cap positions, *i.e.*, increasing the number of substituted Ti more than five, moves the titanium heteroatoms from their natural positions to formation intra-molecular bonding. Hence, these heterofullerenes deform their cage at the Ti—Ti bonds which make them appear cubic-like with the longer Ti—Ti bond lengths (2.872 Å). This phenomenon is occurred in order to reduce their curvature effects and to release their strain energy. The formation of these clusters is quite complicated due to the possibility of high-spin states. According to effort which has been made for global optimization, argument seems rationale for adopting the specific cage structures shown in Figure 1.

3.1. Structural parameters, energy and stability

The average C—C bond distance of C_{20} is from 1.444 to 1.537 Å which enclosures among the bond lengths of ethylene and ethane molecules (1.35, 1.54 Å, respectively) (Tables 1 and 2).

Table 1. The range of bond lengths (Å) calculated for C_{20} and its $C_{20-2n}Ti_nB_n$ heterofullerenes, at B3LYP/AUG-cc-pVTZ.

Species	C=C	Ti–C	B–C	Ti–B	Ti–Ti
C_{20}	1.444-1.537	-	-	-	
$C_{18}Ti_1B_1$	1.423-1.479	2.086	1.571	2.187	-
$C_{16}Ti_2B_2$	1.426-1.471	1.924-2.207	1.527-1.646	2.042-2.151	2.646
$C_{14}Ti_3B_3$	1.371-1.472	1.902-1.912	1.524-1.691	2.002-2.007	
$C_{12}Ti_4B_4$	1.399-1.469	2.064	1.556-1.658	2.247	2.284
$C_{10}Ti_5B_5$	1.450-1.498	2.086-2.133	1.495-1.527	2.093-2.203	-

Table 2. The range of bond angles of C–C–C, C–Ti–C, C–B–C (degree) and θ_{Ti}, θ_B pyramidalization angles (degree) calculated for C_{20} and its $C_{20-2n}Ti_nB_n$ heterofullerenes, at B3LYP/AUG-cc-pVTZ. The pyramidalization angle of C_{20} is θ_C.

Species	C–C–C	C–Ti–C	C–B–C	θ_{Ti}	θ_B
C_{20}	103.99-111.31	-	-	-	-
$C_{18}Ti_1B_1$	103.35-114.23	79.64	100.72	126.59	36.22
$C_{16}Ti_2B_2$	105.23-117.92	-	101.61-102.64	62.15	52.23
$C_{14}Ti_3B_3$	107.70-112.89	83.81-87.40	80.23	61.24	51.16
$C_{12}Ti_4B_4$	109.23-112.34	-	97.96	107.35-131.25	38.06-46.35
$C_{10}Ti_5B_5$	106.21-109.67	39.86-40.89	-	-	-

The substituted doping increases bond lengths of Ti—C, B—C, Ti—B and Ti—Ti to 1.495 Å – 2.646 Å; which are closed to the sum of covalent radii of carbon (0.70 Å), titanium (1.40 Å) and boron (0.85 Å); and decreases bond lengths of C═C to 0.039 Å – 0.073 Å. Also, the bond angles of C—Ti—C and C—B—C are diminished in the range of 39.86° – 87.40° and 80.23° – 102.64°, respectively, *vs.* the range of C–Ĉ–C bond angles of C_{20} from 103.99° to 111.31° (Table 2). The pyramidalization angle on C, Ti and B atoms of C_{20} and $C_{18}Ti_1B_1$ is measured as $\theta_C = 360 - [(C–C–C)_1 + (C–C–C)_2 + (C–C–C)_3]$, $\theta_{Ti} = 360 - [(C–Ti–C)_1 + (C–Ti–B)_2 + (B–Ti–C)_3]$ and $\theta_B = 360 - [(C–B–C)_1 + (C–B–Ti)_2 + (Ti–B–C)_3]$, respectively [23]. Since titanium and boron heteroatoms adopt sp^3 hybridization more than sp^2, these substitutions display higher pyramidalization angle of θ_{Ti} and θ_B than θ_C, and deform their cage around Ti—B bonds. Also, the absolute value of E_{tot} is increased as n of heterofullerenes is increased and the smallest vibrational frequency (υ_{min}) emerges true minimum for them (Table 3).

Table 3. The first thermodynamic parameters including total energies (E_{tot} in *a.u.*), smallest vibrational frequencies (υ_{min} in cm^{-1}), zero-point vibrational energies (ZPVE in kcal/mol) and binding energies (*B.E.* in eV/atom) calculated for C_{20} and its $C_{20-2n}Ti_nB_n$ derivatives with n = 1-5.

Species	E_{tot} [a, (b), c, [d]]	υ_{min} [e]	ZPVE[e]	*B.E.*[d]
C_{20}	-761.60234 (-761.18425) -761.18350 [-761.67038]	82.23	70.84	7.83
$C_{18}Ti_1B_1$	-1559.563072 (-1559.207676) -1559.44292 [-1559.852027]	167.41	66.63	12.25
$C_{16}Ti_2B_2$	-2357.639009 (-2357.316075) -2357.526294 [-2357.997112]	144.46	61.64	18.67
$C_{14}Ti_3B_3$	-3155.677780 (-3155.363587) -3155.555512 [-3156.095962]	106.52	53.84	25.03
$C_{12}Ti_4B_4$	-3953.747407 (-3953.453624) -3953.626146 [-3954.229619]	62.39	51.72	31.44
$C_{10}Ti_5B_5$	-4751.95320 (-4751.704444) -4751.83972 [-4751.900421]	24.24	45.66	38.03

At [a]B3LYP/6-311++G**, [b]M06-2X/6-311++G**, [c]B3PW91/6-311++G**, [d]B3LYP/AUG-cc-pVTZ, and [e]B3LYP/6-311+G*.

Probing the mixed-cage geometries show the reduction of θ_B pyramidalization angles to compensate for the bigger θ_{Ti} pyramidalization angles *and vice versa* (Figure 3).

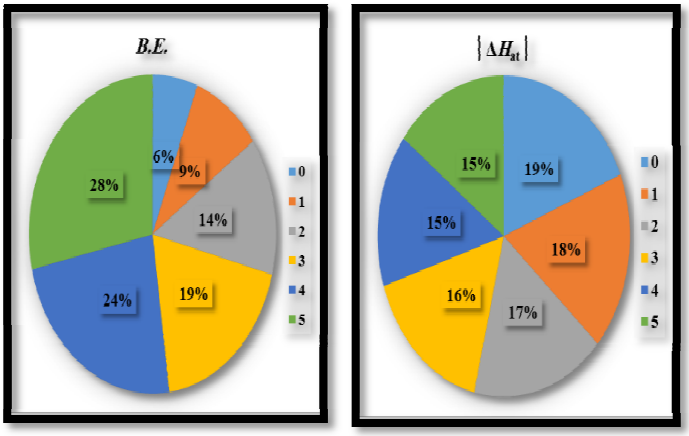

Fig. 3. Comparison of calculated binding energy (*B.E.* in eV/atom), and absolute heat of atomization ($|\Delta H_{at}|$ in kcal/mol) for C_{20} cage (n = 0) and $C_{20-2n}Ti_nB_n$ heterofullerenes (n = 1-5), at B3LYP/6-311+G*.

Substituent effects of titanium and boron on degrees of deformation show differently percentage, as the θ_B pyramidalization angles are smaller than the θ_{Ti} pyramidalization angles. It seems that, from $C_{18}Ti_1B_1$ to $C_{12}Ti_4B_4$; the θ_B angle, tendency of curvature and the released strain energy in the boron sites decreases to compensate for increasing of θ_{Ti} angle, tendency of curvature and the released strain energy in the titanium sites *and vice versa*. Furthermore, due to relief of strain, the bond angles and the θ_{Ti}, θ_B pyramidalization angles are not comparable to each other. Due to the natural sp^2 hybridization of boron, and in order to accommodate the smaller B atoms in the cage structure, all θ_B

pyramidalization angles are smaller than 100° while θ_{Ti} pyramidalization angles are either smaller or bigger than 100°. The $C_{18}Ti_1B_1$, $C_{16}Ti_2B_2$ and $C_{14}Ti_3B_3$ species show the υ_{min} values higher than C_{20} (167.41, 144.46 and 106.52 cm^{-1}, respectively, *vs.* 82.23 cm^{-1}) [24]. Interestingly, there is a rather good consistency between the absolute value of E_{tot}, zero-point vibrational energies (ZPVE) and *B.E.* while n increases. Thus, substituting increases *B.E.* of the scrutinized heterofullerenes (the range of 12.25 eV/atom for $C_{18}Ti_1B_1$ to 38.03 eV/atom for $C_{10}Ti_5B_5$) compared to the unsubstituted cage (7.83 eV/atom) (Figure 4). The frontier molecular orbital's (FMO's) energy splitting has been applied as a criterion of kinetic stability of fullerenes and other nanostructutes. Here, the band gap of structures is differently depending on n and topology of Ti and B substituents (Table 4).

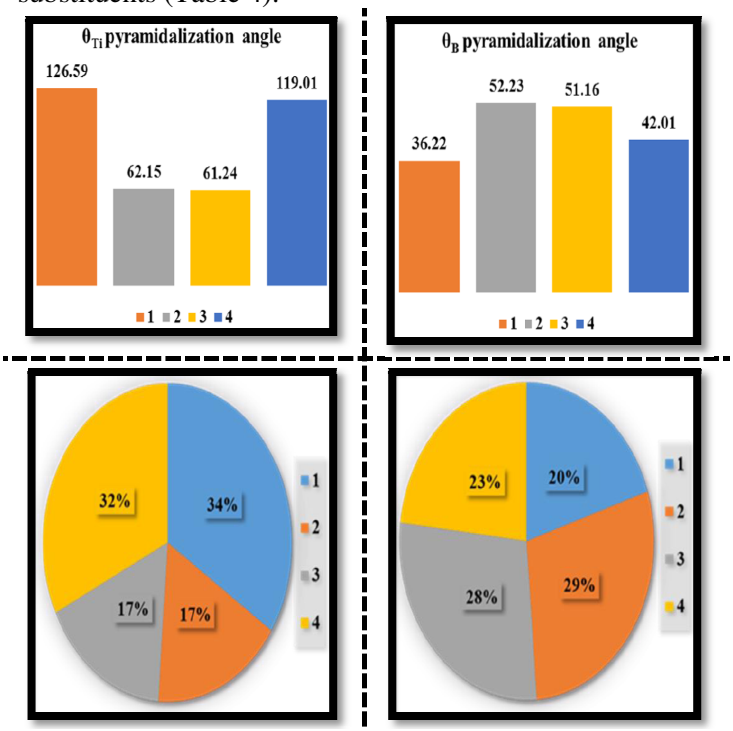

Fig. 4. Substituent effects of titanium (left) and boron (right) on stability of $C_{20-2n}Ti_nB_n$ heterofullerenes *via* comparison of the resulted pyramidalization angles (degree) and n, at B3LYP/AUGcc-pVTZ.

Table 4. The first kinetic parameters including the frontier molecular orbital energies (E_{HOMO} and E_{LUMO} in *a.u.*), along with their band gaps ($\Delta E_{HOMO\text{-}LUMO}$ in eV) calculated for C_{20} and its $C_{20-2n}Ti_nB_n$ heterofullerenic derivatives with n = 1-5.

Species	E_{HOMO} [a, (b), [c]]	E_{LUMO} [a, (b), [c]]	$\Delta E_{HOMO\text{-}LUMO}$ [a, (b), [c]]
C_{20}	-0.20134, (-0.21055) [-0.20455]	-0.13054 (-0.12567) [-0.13351]	1.93 (2.31) [1.93]
$C_{18}Ti_1B_1$	-0.19888 (-0.19898) [-0.20178]	-0.11656 (-0.10724) [-0.11726]	2.24 (2.50) [2.30]
$C_{16}Ti_2B_2$	-0.18848 (-0.19307) [-0.19002]	-0.12314 (-0.11716) [-0.12221]	1.78 (2.07) [1.85]
$C_{14}Ti_3B_3$	-0.17193 (-0.16181) [-0.16149]	-0.09496 (-0.08818) [-0.09599]	2.09 (2.00) [1.78]
$C_{12}Ti_4B_4$	-0.15980 (-0.16426) [-0.16069]	-0.08961 (-0.08456) [-0.08951]	1.91 (2.17) [1.94]
$C_{10}Ti_5B_5$	-0.15961 (-0.16760) [-0.16809]	-0.10512 (-0.10425) [-0.11018]	1.48 (1.72) [1.58]

At [a]B3LYP/AUG-cc-pVTZ, [b]M06-2X/6-311++G**, and [c]B3PW91/6-311+G* levels of theory.

Based on B3LYP/AUG-cc-pVTZ, M06-2X/6-311++G** and B3PW91/6-311+G* calculations, the $\Delta E_{HOMO\text{-}LUMO}$ of C_{20} fullerene is estimated 1.93, 2.31 and 1.93 eV, respectively, while the $\Delta E_{HOMO\text{-}LUMO}$ of $C_{18}Ti_1B_1$ by substituting of one Ti—B unit is changed to 2.24, 2.50 and 2.30 eV, respectively). The substituted titanium and boron heteroatoms simultaneously stabilize the highly strained C_{20} cage by CT. Since the C_{20} cage is isolobal but is not isoelectron to the substituted heterofullerenes, the number of electrons and multiplicity of the ground state is varied from a fullerene to another fullerene. Henceforth, the C_{20}, $C_{16}Ti_2B_2$ and $C_{12}Ti_4B_4$ structures are electronically closed-shell, while $C_{18}Ti_1B_1$, $C_{14}Ti_3B_3$ and $C_{10}Ti_5B_5$ are open-shell.

Moreover, the absolute ΔH_{at} value of heterofullerenes is decreased with increasing n. From an energy perspective, $C_{10}Ti_5B_5$ has the lowest $|\Delta H_{at}|$ and it is the most stable species (Table 5).

Table 5. The second thermodynamic parameters including heat of atomization (ΔH_{at} in kcal/mol), nucleus-independent chemical shifts at cage centers (NICS (0) in ppm), polarity (μ in Debye), as well as isotropic polarizability (<α> in *a.u.*) calculated for C_{20} and its $C_{20-2n}Ti_nB_n$ heterofullerenic derivatives with n = 1-5.

Species	ΔH_{at} [a]	NICS (0) [b]	NICS $(0)_{ZZ}$ [b]	μ [b]	<α> [b]
C_{20}	-3354.96	-23.81	+3.69	0.00	187.27

$C_{18}Ti_1B_1$	-3206.17	-50.83	-71.50	6.02	201.64
$C_{16}Ti_2B_2$	-3055.94	-30.33	-59.84	7.52	258.64
$C_{14}Ti_3B_3$	-2910.88	-17.02	-30.30	1.86	303.31
$C_{12}Ti_4B_4$	-2761.34	+0.93	-10.82	0.00	390.42
$C_{10}Ti_5B_5$	-2612.69	+1.93	+0.02	5.60	353.56

At [a]B3LYP/6-311+G*, [b]B3LYP/AUG-cc-pVTZ.

The C_{20}, $C_{18}Ti_1B_1$, $C_{16}Ti_2B_2$, $C_{14}Ti_3B_3$, $C_{12}Ti_4B_4$ and $C_{10}Ti_5B_5$ species have 6, 9, 14, 19, 24 and 28% *B.E.* character in stability, respectively, while they have approximately similar percentage of $|\Delta H_{at}|$ character in stability in the range of 15% to 19% (Figure 4). From the mixing of the two graphs, the share of *B.E.* is different from the share of $|\Delta H_{at}|$ in thermodynamic stability of C_{20} and $C_{20-2n}Ti_nB_n$ nanocages (Figure 5).

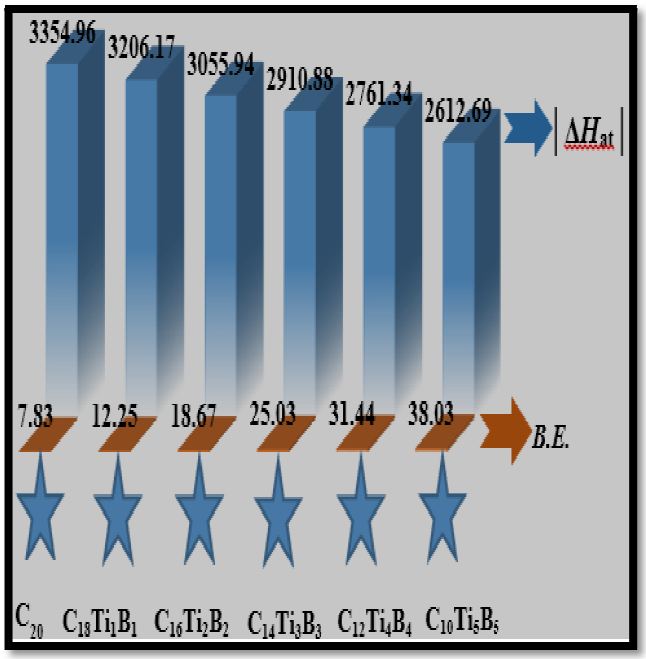

Fig. 5. Comparison of stability *via* calculated *B.E.* (eV/atom), and $|\Delta H_{at}|$ (in kcal/mol) for C_{20} and its $C_{20-2n}Ti_nB_n$ derivatives with n = 1-5, at B3LYP/6-311+G*.

3.2. Aromaticity and charge

Here, we are obtained NICS (0) of C_{20} -23.8 ppm, which implies its strong aromaticity compared to normal benzene and [2.2]paracyclophane molecules; as reference models (-8.5 and -9.5 ppm, respectively). Stacking of two rings to give [2.2]paracyclophane decreases NICS in the inner region. However, in the outer region NICS unexpectedly increases. This increase of NICS in the outer region of [2.2]paracyclophane is likely due to the not completely parallel disposition of the two benzene units in this compound. All the $C_{20-2n}Ti_nB_n$ derivatives show various NICS (0) with range of -50.80 to +1.93 ppm. Thus, $C_{18}Ti_1B_1$, $C_{16}Ti_2B_2$ and $C_{14}Ti_3B_3$ nanocages are aromatic, while $C_{12}Ti_4B_4$ and $C_{10}Ti_5B_5$ nanocages are anti-aromatic. Also, $C_{18}Ti_1B_1$ species exhibits the most negative NICS (0) of -50.80 ppm, among six nanocages. The occupancy of two carbon atoms by one titanium and boron atom, improves the overlap between the nearest carbon atoms with atomic orbitals of substituted dopants indicating the enhanced π-aromaticity (Figure 6).

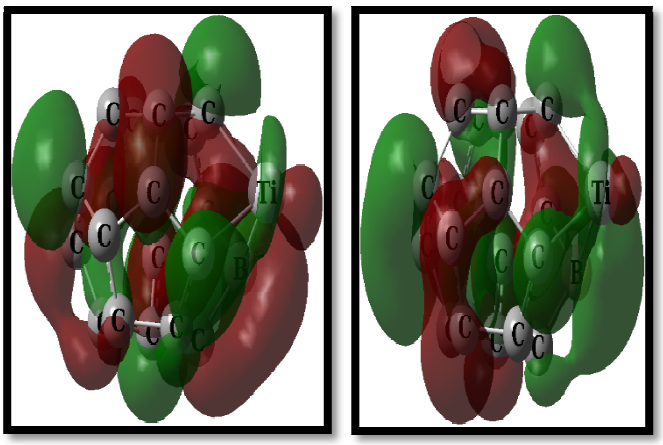

Fig. 6. The shapes of HOMO and LUMO orbitals of $C_{18}Ti_1B_1$.

Table 5 shows the NICS $(0)_{ZZ}$ values better describe the ring current due to the π-electrons as being the out of plane component of NICS. Moreover, all of the scrutinized nanocages display diverse NICS $(0)_{zz}$ with range of -71.50 ppm for $C_{18}Ti_1B_1$ to +0.02 ppm for $C_{10}Ti_5B_5$ which imply strong ring current of $C_{18}Ti_1B_1$, $C_{16}Ti_2B_2$ and $C_{14}Ti_3B_3$ nanocages (-71.50, -59.84 and -30.30, respectively) compared to C_{20} (+3.69 ppm). Though the electronegativity difference is considerable (C: 2.5, Ti: 1.54 and B: 2.0), π-delocalization on the ring perimeter is strengthened in $C_{18}Ti_1B_1$, while such the ring current is weakened in $C_{10}Ti_5B_5$ (Figure 7).

The Ti heteroatoms of $C_{20-2n}Ti_nB_n$ bear varying NBO charges from −0.401 (the most negative charge on carbon atom of $C_{10}Ti_5B_5$) to +1.084 (the most positive charge on titanium atom of $C_{18}Ti_1B_1$ compared to C_{20} (the range of -0.054 to +0.054), at B3PW91/6-311++G** level (Figure 8).

There is a considerable CT from the substituted electropositive Ti heteroatoms to their adjacent electronegative atoms. Boron substitution induces a slight range of positive charge of +0.110 in $C_{10}Ti_5B_5$ to +0.402 in $C_{14}Ti_3B_3$. Clearly, B and C elements inserted in second row of periodic table, which this fact leads to the highest overlap of empty p□orbitals of B heteroatom(s) with π□orbitals of C═C bond.

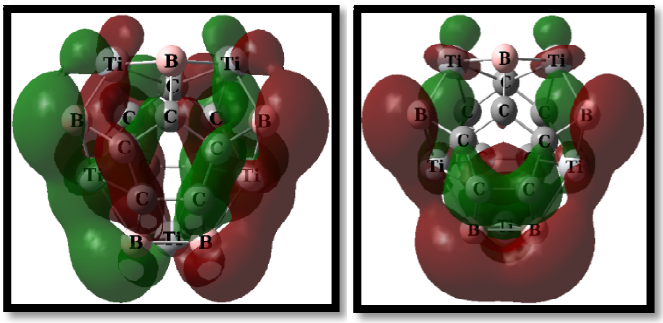

LUMO HOMO

Fig. 7. The shapes of HOMO and LUMO orbitals of $C_{10}Ti_5B_5$.

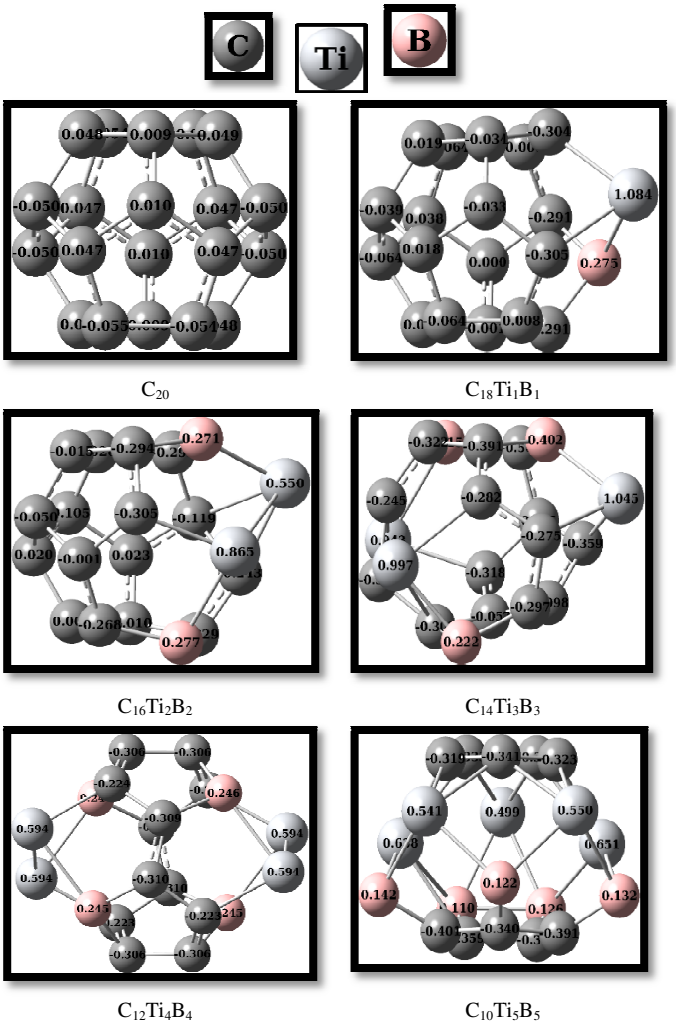

Fig. 8. The NBO atomic charge distribution on C, Ti and B atoms calculated for C_{20} and its $C_{20-2n}Ti_nB_n$ heterofullerenic derivatives with n = 1-5, at B3PW91/6-311++G** level of theory.

Also, Ti atom(s) including electron configuration of $[Ar](4s^2)(3d^2)$, shares two electron with incomplete p□orbital of B atom(s). Hence, there is an overall CT over the surfaces of $C_{20-2n}Ti_nB_n$ especially $C_{18}Ti_1B_1$ compared to C_{20} as the best and as the worst applicant for hydrogen storage, respectively. The MEP plots of the scrutinized heterofullerenes is revealed blue color for titanium sites *via* their positive charge while their negative charge is displayed *via* the red electron cloud in the middle and cap positions for carbon and boron sites. These MEP plots indicate a CT is happened form the Ti heteroatom(s) to the adjacent C and B atoms (Figure 9).

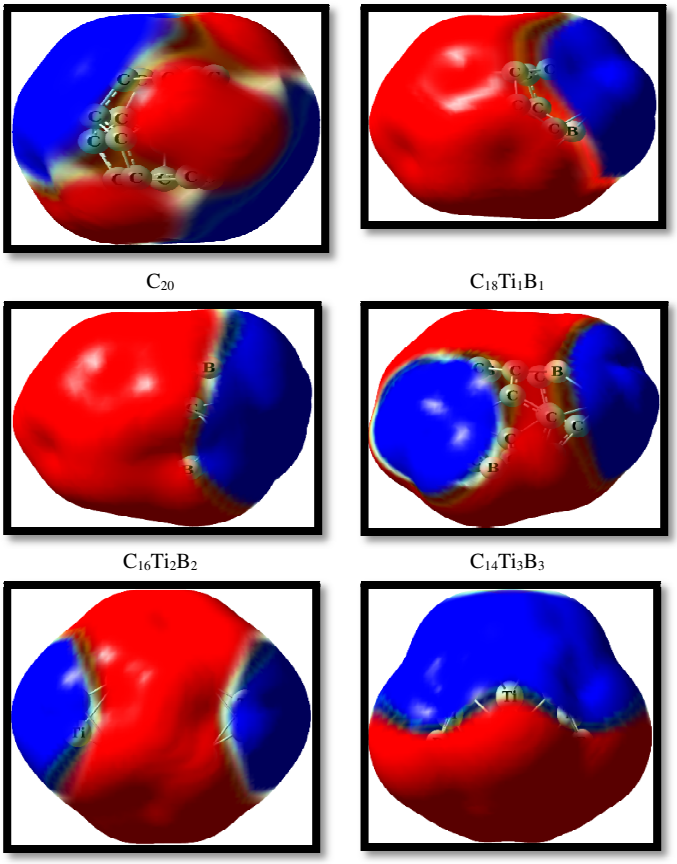

Fig. 9. The resulted MEP maps of C_{20} and its $C_{20-2n}Ti_nB_n$ heterofullerenic derivatives with n = 1-5, at B3PW91/6-311++G** level of theory.

Subsequently, Ti—B substituting leads to considerably dipole moment (7.52, 6.02, 5.60 and 1.86 Debye, for $C_{16}Ti_2B_2$, $C_{18}Ti_1B_1$, $C_{10}Ti_5B_5$ and $C_{14}Ti_3B_3$ structures, respectively) while μ of C_{20} and $C_{12}Ti_4B_4$ cages are zero. The average polarizability; <α>; enlarges from 187.27

a.u. for C_{20} to 390.42 *a.u.* for $C_{12}Ti_4B_4$ molecule. Obviously, four Ti—B substituting units to C_{20} causes to increasing <α> about two times and this species has high activity to polar-polar interaction.

3.3. Reactivity

In this section, the obtained global reactivity of the C_{20} and its substituted $C_{20-2n}Ti_nB_n$ nanocages from FMO's energy is discussed in terms of *N*, ω, μ, η, χ, *S*, along with ΔN_{max}, based on M06-2X/6-311++G** calculations (Table 6).

Table 6. The second kinetic parameters including nucleophilicity index (*N*), global electrophilicity (ω), chemical potential (μ), global hardness (η), electronegativity (χ), global softness (*S*), and also maximum electronic charge (ΔN_{max}) (all in eV) calculated for C_{20} and its $C_{20-2n}Ti_nB_n$ heterofullerenic derivatives with n = 1-5, at M06-2X/6-311++G** level of theory.

Species	*N*	ω	μ	η	χ	*S*	ΔN_{max}
C_{20}	3.73	4.53	-4.57	2.31	4.57	0.22	1.98
$C_{18}Ti_1B_1$	4.05	3.48	-4.17	2.50	4.17	0.20	1.67
$C_{16}Ti_2B_2$	4.21	4.31	-4.22	2.07	4.22	0.24	2.04
$C_{14}Ti_3B_3$	5.06	2.89	-3.40	2.00	3.40	0.25	1.70
$C_{12}Ti_4B_4$	4.99	2.64	-3.39	2.17	3.39	0.23	1.56
$C_{10}Ti_5B_5$	4.90	3.97	-3.70	1.72	3.70	0.29	2.15

Substituting of one to five Ti and B—heteroatoms lead to distinctive variations of *N*, ω, μ, η, χ, *S* and ΔN_{max}. So that, one substituted Ti—B nanocage is considered as the least reactive species, it has the lowest value of *N*, *S* and the highest χ, η and absolute value of μ. Then, it is the most chemically stable species. Due to significant CT from maximum number of titanium and boron heteroatoms to neighboring carbons of $C_{10}Ti_5B_5$, it as the most reactive species, shows the lowest μ and the highest *S* between the scrutinized heterofullerenes.

3.4. NBO analysis

Here, NBO analysis is completed on kinetically stable $C_{18}Ti_1B_1$ nanocage, at the B3PW91/6-311++G** level (Tables 7 and 8).

Table 7. The resulted NBO analysis of B3PW91/6-311++G** calculations for the $C_{18}Ti_1B_1$ heterofullerene.

Bond (A-B)	Occup.	ED_A (%)	ED_B (%)	NBO
$\pi_{C=C}$	0.987	50.01	49.99	$0.707*sp^{2.01}$ $+0.707*sp^{2.05}$
σ_{C-B}	0.976	69.65	30.35	$0.834*sp^{1.52}$ $+0.551*sp^{1.99}$
σ_{Ti-B}	0.980	46.78	53.22	$0.684*sp^{0.33}d^{4.2}$ $+0.729*sp^{1.78}$
$LP(1)_{Ti}$	0.914			$sp^{0.01}d^{99.99}$

Table 8. The hybridization analysis of B3PW91/6-311++G** calculations for the $C_{18}Ti_1B_1$ heterofullerene.

Bond (A-B)	s (%)	p (%)	d (%)
$\pi_{C=C}$	33.23, 32.77	66.67, 67.15	
σ_{C-B}	39.58, 33.46	60.34, 66.50	
σ_{Ti-B}	18.21, 35.98	6.03,64.00	75.75, 0.02
$LP(1)_{Ti}$	0.00	0.01	99.99

The first two columns give orbital and occupancy between 0.987 electrons for C═C bonding orbitals with sp^2 hybrid *vs.* 0.914 electrons for $LP(1)_{Ti}$ with $sp^{0.01}d^{99.99}$ hybrid. The latter hybrid on lone pair of Ti has 99.99% d-character. While, occupancy of σ_{C-B} and σ_{Ti-B} is 0.976 and 0.980 electrons, with $0.834*sp^{1.52}+0.551*sp^{1.99}$ and $0.684*sp^{0.33}d^{4.2}+0.729*sp^{1.78}$ hybrids, respectively.

The bonding orbital of σ_{C-B} shows 69.65% carbon character in $sp^{1.5}$ hybrid and 30.35% boron character in $sp^{1.99}$ hybrid. Also, σ_{Ti-B} bonding orbital exhibits 46.78% titanium character in $sp^{0.33}d^{4.2}$ hybrid and 53.22% boron character in $sp^{1.78}$ hybrid.

Clearly, titanium heteroatom shows lower percentage of NBO and polarization coefficient than the bonding bonds of $\pi_{C=C}$ and σ_{C-B} because it has lower electronegativity than carbon and boron atoms.

Here, 0.834, 0.551, 0.684 and 0.729 are polarization coefficients.

The magnitude of these coefficients reveals the importance of two hybrids in one bond. The order of polarization coefficients is arranged by carbon more than boron and boron more than titanium. In fact, the intermolecular interaction is formed by the suitable overlap between bonding orbital of $\pi_{C=C}$ with anti-bonding orbital of LP^*_{Ti}, LP^*_B and σ^*_{Ti-B}, which results

a CT from donating orbital (with a reducing of its occupancy) to accepting orbital (with a rising of its occupancy).

The intermolecular interaction is happened from different hybrids on their atoms with different percentage of s, p and d orbitals. The most important of donor and acceptor is related to $\pi_{C=C} \rightarrow LP^*(1)_B$, $\pi_{C=C} \rightarrow LP^*(\text{ϒ})_B$, $\pi_{C=C} \rightarrow LP^*(1)_{Ti}$, $\pi_{C=C} \rightarrow LP^*(\text{ϒ})_{Ti}$ and $\pi_{C=C} \rightarrow \sigma^*_{Ti-B}$ interactions and their corresponding energies is 28.32, 12.53, 4.54, 2.10 and 1.15 kcal/mol, respectively (Table 9).

Table 9. The calculated second order perturbation energies $E^{(2)}$ corresponding to the most important charge transfer interactions (donor-acceptor) of $C_{18}Ti_1B_1$, at B3PW91/6-311++G**.

Donor NBO (i)	Acceptor NBO (j)	$E^{(2)}$ (kcal/mol)	E(j) – E(i) (*a.u.*)	F (i,j) (*a.u.*)
$\pi_{C=C}$	$LP^*(1)_B$	28.32	0.39	0.42
$\pi_{C=C}$	$LP^*(2)_B$	12.53	0.28	0.078
$\pi_{C=C}$	$LP^*(1)_{Ti}$	4.54	0.21	0.042
$\pi_{C=C}$	$LP^*(2)_{Ti}$	2.10	0.19	0.025
$\pi_{C=C}$	σ^*_{Ti-B}	1.15	0.34	0.029

4. Conclusion

In this computational research, based on full optimized geometries, none of C_{20} and its $C_{20-2n}Ti_nB_n$ derivatives collapses to deformed open-cage as segregated nanostructure. Isolating Ti—B bonds *via* C═C bond or one C atom is a proper approach for achieving substituted heterofullerene such $C_{10}Ti_5B_5$ since it avoids from five weak homo bonds of Ti—Ti and B—B. The vibrational frequency analysis is applied to assure that all optimized nanocges show no imaginary frequency as true minima. The range of calculated *B.E.* from 12.25 to 38.03 eV/atom reveals the $C_{20-2n}Ti_nB_n$ nanocages are as more thermodynamically stable heterofullerene and better candidate for hydrogen storage than the Ti-decorated B_{38} nanofullerene with *B.E.* of 5.67 eV/atom. Here, the absolute heat of atomization of heterofullerenes decreases as number of substituting Ti—B unit increases. Also, DFT calculations based on B3LYP/AUG-cc-pVTZ, M06-2X/6-311++G** and B3PW91/6-311+G* implies that the band gap as well as conductivity of $C_{20-2n}Ti_nB_n$ structures is variously depending on number and topology of Ti and B heteroatoms. The obtained NICS (0) data indicates that substituting C_{20} to $C_{18}Ti_1B_1$, $C_{16}Ti_2B_2$ and $C_{14}Ti_3B_3$ leads to considerably more aromaticity character than benzene, [2.2]paracyclophane and C_{20} molecules while $C_{12}Ti_4B_4$ and $C_{10}Ti_5B_5$ nanocages exhibit anti-aromaticity character. High NBO charge dispersion on $C_{20-2n}Ti_nB_n$ surfaces with range of −0.401 on carbon atom of $C_{10}Ti_5B_5$ to +1.084 on titanium atom of $C_{18}Ti_1B_1$ compared to C_{20} with range of -0.054 to +0.054, leads to high *B.E.* of H_2 molecule in its absorption on the $C_{18}Ti_1B_1$ heterofullerene and causes more exploration on its probable appliance for hydrogen storage. The blue colored MEP images reveal the positive charge on Ti sites, red colored MEP images display the negative charge on C and B sites, demonstrating a suitable CT is occurred form Ti substitutions to the neighboring C and B atoms. The <α> value increases from 187.27 *a.u.* for C_{20} to 390.42 *a.u.* for $C_{12}Ti_4B_4$ species. Obviously, this species exhibits high activity to polar-polar interaction. Also, the global reactivity of C_{20} and its $C_{20-2n}Ti_nB_n$ derivatives is increased as the number of substituted Ti and B dopants (n) is increased. Hence, $C_{18}Ti_1B_1$ as the least chemical reactive species, shows the lowest N, S and the highest χ, η and absolute value of μ. The NBO analysis on $C_{18}Ti_1B_1$ indicates large CT is take placed from its $\pi_{C=C}$ bonds to their neighboring LP^*_B, LP^*_{Ti} and σ^*_{Ti-B} anti-bonds.

Acknowledgements

Authors state that no fund is used in this research.

References

[1] (a) T. M. Simeon, I. Yanov, J. Leszczynski, *Ab initio* quantum chemical studies of fullerene molecules with substitutes $C_{59}X$. [X = Si, Ge, Sn], $C_{59}X^-$ [X = B, Al, Ga, In], and $C_{59}X^+$ [X = N, P, As, Sb]. Int. J. Quantum. Chem. 105 (2005) 429. (b) Z. Chen, R. B. King, Spherical aromaticity: recent work on fullerenes, polyhedral boranes, and related structures. Chem. Rev. 105 (2005) 3613. (c) O. Vostrowsky, A. Hirsch, Heterofullerenes. Chem. Rev. 106 (2006) 5191. (d) I. Zanella, A. Fazzio, A. J. R. da Silva, $C_{59}Si$ on the Monohydride Si (100): H–(2× 1) Surface. J. Phys. Chem. B 110 (2006) 10849. (e) C. Massobrio, D. M. Djimbi, M. Matsubara, R. Scipioni, M. Boero, Stability of $Ge_{12}C_{48}$ and $Ge_{20}C_{40}$ heterofullerenes: A first principles molecular dynamics study. Chem. Phys. Lett. 556 (2013) 163. (f) L. Koponen, M. J. Puska, R. M. Nieminen, Photoabsorption spectra of small fullerenes and Si-heterofullerenes. J Chem Phys 128 (2008) 154307.

[2] (a) T. Akasaka, F. Wudl, S. Nagase, Chemistry of Nanocarbons. Angew. Chem. Int. Ed. 50 (2011) 4048. (b) O. Vostrowsky, A. Hirsch, Heterofullerenes. Chem. Rev. 106 (2006) 5191. (c) N. Lou, Y. Li, C. Cui, Y. Liu, L. Gan, Preparation of Azafullerene $C_{59}NR_5$ and Fullerene Derivative $C_{60}NAr_5$ with a Pyridine Moiety on the Cage Skeleton. Org. Lett. 18 (2016) 2236. (d) Y. Hashikawa, M. Murata, A. Wakamiya, Y. Murata, Synthesis and Properties of

Endohedral Aza[60]fullerenes: $H_2O@C_{59}N$ and $H_2@C_{59}N$ as Their Dimers and Monomers. J. Am. Chem. Soc. 138 (2016) 4096. (e) L. Martín-Gomis, G. Rotas, K. Ohkubo, F. Fernández-Lázaro, S. Fukuzumi, N. Tagmatarchis, Á. Sastre-Santos, Does a nitrogen matter? Synthesis and photoinduced electron transfer of perylenediimide donors covalently linked to $C_{59}N$ and C_{60} acceptors. Nanoscale 7 (2015) 7437. (f) W. Cambarau, U. F. Fritze, A. Viterisi, E. Palomares, M. von Delius, Increased short circuit current in an azafullerene-based organic solar cell. Chem Commun 51 (2015) 1128. (g) C. D. Wessendorf, R. Eigler, S. Eigler, J. Hanisch, A. Hirsch, E. Ahlswede, Investigation of pentaarylazafullerenes as acceptor systems for bulk-heterojunction organic solar cells. Sol. Energy Mater. Sol. Cells 132 (2015) 450.

[3] (a) K. S. Novoselov, A. K. Geim, S. V. Morozov, D. Jiang, Y. Zhang, S. V. Dubonos, I. V. Grigorieva, A. A. Firsov, Electric field effect in atomically thin carbon films. Science 306 (5696) (2004) 666. (b) H. W. Kroto, J. R. Heath, S. C. O'Brien, R. F. Curl, R. E. Smalley, C_{60}: Buckminsterfullerene. Nature 318 (1985) 162. (c) A. Mujica, A. Rubio, A. Munoz, R. J. Needs, High-pressure phases of group IV, III–V, and II–VI compounds. Rev. Mod. Phys. 75 (2003) 863. (d) W. J. Chao, R. Kosugi, J. Senzaki, K. Fukuda, K. Arai, S. Suzuki, New High-k $SrTa_2O_6$ Gate Dielectrics Prepared by Plasma-Enhanced Atomic Layer Chemical Vapor Deposition. Appl. Phys. Lett. 77 (2000) 2054. (e) P. Schwerdtfeger, L. N. Wirz, J. Avery, The topology of fullerenes. WIREs Comput. Mol. Sci. 5 (2015) 96. (f) X. Lu, Z. Chen, Curved π-conjugation, aromaticity, and the related chemistry of small fullerenes (< C_{60}) and single-walled carbon nanotubes. Chem. Rev. 105 (2005) 3643.

[4] (a) H. Dong, T. Hou, S. T. Lee, Y. Y. Li, New Ti-decorated B_{40} fullerene as a promising hydrogen storage material, Sci. Rep. 5 (2015) 9952. (b) Q. L. Lu, S. G. Huang, Y. D. Li, J. G. Wan, Q. Q. Luo, Alkali and alkalineearth atom-decorated B_{38} fullerenes and their potential for hydrogen storage. Int. J. Hydrogen Energy 40(38) (2015) 13022. (c) N. G. Szwacki, A. Sadrzadeh, B. I. Yakobson, B_{80} fullerene: an *ab initio* prediction of geometry, stability, and electronic structure. Phys. Rev. Lett. 98 (2007) 166804. (d) C. Özdogan, S. Mukhopadhyay, W. Hayami, Z. B. Güvenc, R. Pandey, I. Boustani, The unusually stable B_{100} fullerene, structural transitions in boron nanostructures, and a comparative study of a-and g-boron and sheets. J. Phys. Chem. C 114 (2010) 4362. (e) Q. B. Yan, X. L. Sheng, Q. R. Zheng, L. Z. Zhang, G. Su, Family of boron fullerenes: general constructing schemes, electron counting rule, and *ab initio* calculations. Phys. Rev. B 78 (2008) 201401.

[5] (a) J. T. Muya, G. Gopakumar, M. T. Nguyen, A. Ceulemans, The leapfrog principle for boron fullerenes: a theoretical study of structures and stability of B_{112}. Phys. Chem. Chem. Phys. 13 (2011) 7524. (b) T. BaáTai, M. ThoáNguyen, A new chiral boron cluster B_{44} containing nonagonal holes. Chem. Commun. 52 (2016) 1653. (c) Y. J. Wang, Y. F. Zhao, W. L. Li, T. Jian, Q. Chen, X. R. You, T. Ou, X. Y. Zhao, H. J. Zhai, S. D. Li, J. Li, L. S. Wang, Observation and characterization of the smallest borospherene. B_{28}^- and B_{28}. J. Chem. Phys. 144 (2016) 064307. (d) N. G. Szwacki, Boron fullerenes: a first-principles study. Nanoscale Res. Lett. 3 (2008) 49. (e) X. L. Sheng, Q. B. Yan, Q. R. Zheng, G. Su, Boron fullerenes B_{32} 8k with four-membered rings and B_{32} solid phases: geometrical structures and electronic properties. Chem. Chem. Phys. 11 (2009) 9696.

[6] (a) L. Wang, J. Zhao, F. Li, Z. F. Chen, Boron fullerenes with 32-56 atoms: irregular cage configurations and electronic properties. Chem. Phys. Lett. 501 (2010) 16. (b) R. R. Zope, T. Baruah, K. C. Lau, A. Y. Liu, M. R. Pederson, B. I. Dunlap, Boron fullerenes: from B_{80} to hole doped boron sheets. Phys. Rev. B 79 (2009) 161403. (c) Y. Li, G. Zhou, J. Li, B. L. Gu, W. H. Duan, Alkali-metal-doped B_{80} as high-capacity hydrogen storage media. J. Phys. Chem. C 112 (2008) 19268. (d) M. Li, Y. Li, Z. Zhou, P. Shen, Z. Chen, Ca-coated boron fullerenes and nanotubes as superior hydrogen storage materials. Nano Lett. 9 (2009) 1944. (e) Y. F. Zhao, M. T. Lusk, A. C. Dillon, M. J. Heben, S. B. Zhang, Boronbased organometallic nanostructures: hydrogen storage properties and structure stability. Nano Lett. 8 (2008) 157. (f) J. L. Li, Z. S. Hu, G. W. Yang, High-capacity hydrogen storage of magnesium-decorated boron fullerene. Chem. Phys. 392 (2012) 16.

[7] (a) W. W. Wu, Z. Y. Tian, S. L. Dong, Yttrium-dispersed B_{80} fullerenes: promising materials for hydrogen storage. Eur. Phys. J. 109 (2015) 56004. (b) G. Wu, J. Wang, X. Zhang, L. Zhu, Hydrogen storage on metalcoated B_{80} buckyballs with density functional theory. J. Phys. Chem. C 113 (2009) 7052. (c) E. Durgun, S. Ciraci, W. Zhou, T. Yildirim, Transition-metalethylene complexes as high-capacity hydrogen-storage media. Phys. Rev. Lett. 97 (2006) 226102. (d) A. S. Shalabi, S. A. Aal, M. M. Assem, W. S. Abdel Halim, *Ab initio* characterization of Ti decorated SWCNT for hydrogen storage. Int. J. Hydrogen Energy 38 (2013) 140.

[8] (a) S. Barman, P. Sen, G. P. Das, Ti-decorated doped silicon fullerene: a possible hydrogen-storage material. J. Phys. Chem. C 112 (2008) 19963. (b) Q. X. Bao, H. Zhang, S. W. Gao, X. D. Li, X. L. Cheng, Hydrogen adsorption on Ti containing organometallic structures grafted on silsesquioxanes. Struct. Chem. 21 (2010) 1111. (c) C. Tang, S. Chen, W. Zhu, J. Kang, X. He, Z. J. Zhang, Transition metal Ti coated porous fullerene $C_{24}B^{24}$: potential material for hydrogen storage. Int. J. Hydrogen Energy 40 (2015) 16271. (d) A. Lebon, J. Carrete, L. J. Gallego, A. Vega, Ti-decorated zigzag graphene nanoribbons for hydrogen storage. A van der Waals-corrected density-functional study. Int. J. Hydrogen Energy 40 (2015) 4960. (e) Q. Sun, Q. Wang, P. Jena, Y. Kawazoe, Clustering of Ti on a C_{60} surface and its effect on hydrogen storage. J Am Chem Soc 127 (2005) 14582.

[9] (a) M. Koohi, S. Soleimani-Amiri, M. Shariati, Novel X- and Y-substituted heterofullerenes $X_4Y_4C_{12}$ developed from the nanocage C_{20}, where X = B, Al, Ga, Si and Y = N, P, As, Ge: a comparative investigation on their structural, stability, and electronic properties at DFT. Struct. Chem. 29(3) (2018) 909. (b) M. T. Baei, M. Koohi, M. Shariati, Characterization

of C_{20} fullerene and its isolated $C_{20-n}Ge_n$ derivatives (n = 1-5) by alternating germanium atom(s) in equatorial position: A DFT survey. Heteroatom Chem. 29 (2018) e21410. (c) M. T. Baei, M. Koohi, M. Shariati, Structure, stability, and electronic properties of AlP nanocages evolved from the world's smallest caged fullerene C_{20}: A computational study at DFT. J. Mol. Struct. 1159 (2018) 118. (d) S. Soleimani Amiri, M. Koohi, B. Mirza, Characterizations of B, and N heteroatoms as substitutional doping on structure, stability, and aromaticity of novel heterofullerenesevolvedfrom the smallest fullerene cage C_{20}: A density functional theory perspective. J. Phys. Org. Chem. 29 (2016) 514. (e) M. Koohi, S. Soleimani Amiri, B. N. Haerizade, Substituent effect on structure, stability and aromaticity of novel $B_nN_mC_{20-(n+m)}$ heterofullerenes. J. Phys. Org. Chem. 30 (2017) e3682. (f) M. Koohi, M. Z. Kassaee, M. Ghavami, B. N. Haerizade, A. A. Ahmadi, $C_{20-n}Ge_n$ heterofullerenes (n = 5 - 10) on focus: a density functional perspective. Monatsh. Chem. 146 (2015) 1409. (g) M. Koohi, S. Soleimani Amiri, M. Shariati, Silicon impacts on structure, stability and aromaticity of $C_{20-n}Si_n$ heterofullerenes (n = 1 - 10): a density functional perspective. J. Mol. Struct. 1127 (2017) 522. (h) M. Koohi, M. Shariati, S. Soleimani Amiri, A comparative study on the Ge_6C_{14} heterofullerene nanocages: a density functional survey. J. Phys. Org. Chem. 30 (2017) e3678. (i) S. Soleimani-Amiri, M. Koohi, Z. Azizi, Characterization of nonsegregated $C_{17}Si_3$ heterofullerenic isomers using density functional theory method. J Chin Chem Soc 65 (2018) 1453.

[10] (a) R. Tawfeeq Kareem, Z. Rahmani, S. Ebrahimiasl, A. Ebadi, Z. Rostami Characterization of titanium influences on structure and thermodynamic stability of novel $C_{20-n}Ti_n$ nanofullerenes (n = 1 - 5): A density functional perspective. J. Mol. Model. 27(6) (2021) 176. (b) R. T. Kareem, S. Ahmadi, Z. Rahmani, A. G. Ebadi, S. Ebrahimiasl, Characterization of titanium influences on structure and thermodynamic stability of novel $C_{20-n}Ti_n$ nanofullerenes (n=1-5): a density functional perspective. J. Mol. Model. 27(6) (2021) 176. (c) E. Vessally, M. D. Esrafili, R. Nurazar, P. Nematollahi, A. Bekhradnia, A DFT study on electronic and optical properties of aspirin–functionalized $B_{12}N_{12}$ fullerene–like nanocluster. Struct. Chem. 28 (2017) 735. (d) E. Vessally, E. Ahmadi, S. Alibabaei, M. D. Esrafili, A.Hosseinian, Adsorption and decomposition of formaldehyde on the $B_{12}N_{12}$ nanostructure: a density functional theory study. Monatsh. Chem. 148 (2017) 1727.

[11] (a) S. A. Siadati, E. Vessally, A. Hosseinian, L. Edjlali, Possibility of sensing, adsorbing, and destructing the Tabun–2D–skeletal (Tabun nerve agent) by C_{20} fullerene and its boron and nitrogen doped derivatives. Synthetic Met 220 (2016) 606. (b) E. Vessally, S. A. Siadati, A. Hosseinian, L. Edjlali, Selective sensing of ozone and the chemically active gaseous species of the troposphere by using the C_{20} fullerene and graphene segment. Talanta 162 (2017) 505. (c) E. Vessally, S. Soleimani–Amiri, A. Hosseinian, L. Edjlali, A. Bekhradnia, The Hartree–Fock exchange effect on the CO adsorption by the boron nitride nanocage. Physica E 87 (2017) 308. (d) K. Nejati, A. Hosseinian, E. Vessally, A. Bekhradnia, L. Edjlali, A comparative DFT study on the interaction of cathinone drug with BN nanotubes, nanocages, and nanosheets. Appl. Surf. Sci. 422 (2017) 763. (e) A. Hosseinian, E. Vessally, A. Bekhradnia, K. Nejati, G. Rahimpour, Benzoylethanamine drug interaction with the AlN nanosheet, nanotube and nanocage: Density functional theory studies. Thin Solid Films 640 (2017) 93.

[12] (a) A. Hosseinian, A. Bekhradnia, E. Vessally, L. Edjlali, M. D. Esrafili, A DFT study on the central–ring doped HBC nanographenes. J. Mol. Graph. Model. 73 (2017) 101. (b) A. Hosseinian, Z. Asadi, L. Edjlali, A. Bekhradnia, E. Vessally, NO_2 sensing properties of a borazine doped nanographene: A DFT study. Comput. Theor. Chem. 1106 (2017) 36. (c) K. Nejati, A. Hosseinian, A. Bekhradnia, E. Vessally, L. Edjlali, Na–ion batteries based on the inorganic BN nanocluster anodes: DFT studies. J. Mol. Graph. Model. 74 (2017) 1. (d) B. Mirza, S. Soleimani-Amiri, M. Mirza, Reaching for $[6]_n$ SiC-cyclacenes and $[6]_n$ SiC-acenes: A DFT approach. J. Phys. Org. Chem. 31 (2017) 3754. (e) E. Vessally, S. Soleimani–Amiri, A. Hosseinian, L. Edjlali, A. Bekhradnia, A comparative computational study on the BN ring doped nanographenes. Appl. Surf. Sci. 396 (2017) 740. (f) K. Nejati, A. Hosseinian, L. Edjlali, E. Vessally, The effect of structural curvature on the cell voltage of BN nanotube based Na–ion batteries. J. Mol. Liq. 229 (2017) 167. (g) L. Safari, E. Vessally, A. Bekhradnia, A. Hosseinian, L. Edjlali, A DFT study on the sensitivity of two–dimensional BN nanosheet to nerve agents cyclosarin and tabun. Thin Solid Films, 623 (2017) 157. (d) M. Koohi, H. Bastami, Structure, stability, MEP, NICS, reactivity, and NBO of Si—Ge nanocages evolved from C_{20} fullerene at DFT. Monatshefte für Chemie – Chem. Mont. 151 (2020) 693.

[13] (a) E. Vessally, F. Behmagham, B. Massoumi, A. Hosseinian, L. Edjlali, Carbon nanocone as an electronic sensor for HCl gas: Quantum chemical analysis. Vacuum, 134 (2016) 40. (b) S. Bashiri, E. Vessally, A. Bekhradnia, A. Hosseinian, L. Edjlali, Utility of extrinsic [60] fullerenes as work function type sensors for amphetamine drug detection: DFT studies. Vacuum, 136 (2017) 156. (c) F. Behmagham, E. Vessally, B. Massoumi, A. Hosseinian, L. Edjlali, A computational study on the SO_2 adsorption by the pristine, Al, and Si doped BN nanosheets, Superlattices Microstruct. 100 (2016) 350. (d) M. Koohi, M. Ghavami, B. N. Haerizade, H. Zandi, M. Z. Kassaee, Cyclacenes and short zigzag nanotubes with alternanting Ge—C bonds: theoretical impacts of Ge on the ground state, strain, and band gap. J. Phys. Org. Chem. 27 (2014) 735.

[14] (a) A. D. Becke, Density-functional exchange-energy approximation with correct asymptotic behavior, Phys. Rev. A 38 (1988) 3098. (b) A. D. J. Becke, Density□functional thermochemistry. III. The role of exact exchange, Chem. Phys. 98 (1993) 5648. (c) C. Lee, W. Yang, R. G. Parr, Development of the Colle-Salvetti correlation-energy formula into a functional of the electron density, Phys. Rev. B 37 (1988) 785. (d) A. D. Becke, Density□functional thermochemistry. IV. A new dynamical correlation functional and implications for exact□exchange mixing, J. Chem. Phys. 104 (1996) 1040.

[15] (a) M. W. Schmidt, K. K. Baldridge, J. A. Boatz, S. T. Elbert, M. S. Gordon, J. H. Jensen, S. Koseki, N. Matsunaga, K. A. Nguyen, S. J. Su, T. L. Windus, M. Dupuis, J. A. Montgomery, General atomic and molecular electronic structure system, J. Comput. Chem., 14 (11) (1993) 1347. (b) A. L. Sobolewski, W. Domcke, *Ab Initio* Investigation of the Structure and Spectroscopy of Hydronium–Water Clusters, J. Phys. Chem. A 106 (2002) 4158.

[16] Y. Zhao, D. G. Truhlar, The M06 suite of density functionals for main group thermochemistry, thermochemical kinetics, noncovalent interactions, excited states, and transition elements: two new functionals and systematic testing of four M06-class functionals and 12 other functionals, Theor. Chem. Account. 120 (2008) 215.

[17] (a) W. J. Hehre, L. Radom, P. v. R. Schleyer, J. A. Pople, *Ab Initio* Molecular Orbital Theory, John Wiley & Sons, New York (1986). (b) J. B. Foresman, A. Frisch, Exploring Chemistry with Electronic structure Methods, Gaussian, Inc., Pittsburgh. PA (1996). (c) P. C. Hariharan, J. A. Pople, Accuracy of AH, equilibrium geometries by single determinant molecular orbital theory. J. Mod. Phys. 27 (1974) 209. (d) M. M. Francl, W. J. Pietro, W. J. Hehre, J. S. Binkley, M. S. Gordon, D. J. DeFrees, J. A. Pople, Self-Consistent Molecular Orbital Methods. XXIII. A Polarization-Type Basis Set for Second Row Elements, J. Chem. Phys. 77 (1982) 3654. (e) M. J. Frisch, J. A. Pople, J. S. Binkley, Self-Consistent Molecular Orbital Methods 25: Supplementary Functions for Gaussian Basis Sets, J. Chem. Phys. 80 (1984) 3265. (f) T. Clark, J. Chandrasekhar, G. W. Spitznagel, P.v.R. Schleyer, Efficient diffuse function-augmented basis sets for Anion Calculations. III. The 3-21+G set for first-row elements, Li-F, J. Comput. Chem. 4 (1983) 294.

[18] (a) F. Weinhold, E. D. Glendening, NBO 7.0 Program Manual Natural Bond Orbital Analysis Programs. J. Comput. Chem. 33 (2012) 2363. (b) F. Weinhold, Natural Bond Orbital Analysis: A Critical Overview of Relationships to Alternative Bonding Perspectives. J. Comput. Chem. 33 (2012) 2363. (c) E. D. Glendening, C. R. Landis, F. Weinhold, Natural bond orbital methods. Wiley Interdiscip. Rev. Comput. Mol. Sci. 2 (2012) 1. (d) G. Zhang, C. B. Musgrave, Comparison of DFT Methods for Molecular Orbital Eigenvalue Calculations. J. Phys. Chem. A 111 (2007) 1554.

[19] (a) R. Krishna, M. J. Frisch, J. A. Pople, Contribution of Triple Substitutions to the Electron Correlation Energy in Fourth Order Perturbation Theory. J. Chem. Phys. 72 (1980) 4244. (b) R. A. Kendall, T. H. Jr. Dunning, R. J. Harrison, Electron affinities of the first□row atoms revisited. Systematic basis sets and wave functions. J. Chem. Phys. 96 (1992) 6796. (c) J. P. Predew, Y. Wang, Accurate and simple analytic representation of the electron-gas correlation energy. Phys. Rev. B 45 (1992) 13244.

[20] (a) P. v. R. Schleyer, C. Maerker, A. Dransfeld, H. Jiao, N. J. R. van Eikema Hommes, Nucleus-independent chemical shifts (NICS): a simple and efficient aromaticity probe. J. Am. Chem. Soc. 118 (1996) 6317. (b) P. v. R. Schleyer, H. Jiao, N. J. R. van Eikema Hommes, V. G. Malkin, O. L. Malkina, An evolution of the aromaticity of inorganic rings: refined evidence from magnetic properties. J Am Chem Soc 119 (1997) 12669. (c) P. v. R. Schleyer, M. Manoharan, Z. Wang, B. Kiran, H. Jiao, R. Puchta, N. J. R. van Eikema Hommes, Dissected nucleus-independent chemical shift analysis of p-aromaticity and antiaromaticity. Org. Lett. 3(16) (2001) 2465.

[21] (a) M. R. Ibrahim, P. v. R. Schleyer, Atom Equivalents for Relating *Ab Initio* Energies to Enthalpies of Formation. J. Comput. Chem. 6 (1985) 157. (b) N. Mizorogi, J.-I. Aihara, PM3 localization energies for the isolated-pentagon isomers of the C_{84} fullerene. Phys. Chem. Chem. Phys. 5 (2003) 3368. (c) M. Watanabe, D. Ishimaru, N. Mizorogi, M. Kiuchi, J.-I. Aihara, Thermodynamically and kinetically stable isomers of the C_{88} and C_{90} fullerenes. J. Mol. Struct. (THEOCHEM) 726 (2005) 11. (d) Z. Yang, X. Xu, G. Wang, Z. Shang, Z. Cai, Y. Pan, X. Zhao, A systematic investigation on the molecular behaviors of substituted fullerenes $C_{34}X_2$ (X = N, B). J. Mol. Struct. (THEOCHEM) 618 (2002) 191.

[22] (a) L. R. Domingo, E. Chamorro, P. Pérez, Understanding the Reactivity of Captodative Ethylenes in Polar Cycloaddition Reactions. A Theoretical Study. J Org Chem 73 (2008) 4615. (b) R. G. Parr, L. Szentpaly, S. Liu, Electrophilicity Index. J. Am. Chem. Soc. 121 (1999) 1922. (c) R. G. Pearson Absolute electronegativity and hardness: applications to organic chemistry. J. Org. Chem. 54 (1989) 1423. (d) P. K. Chattaraj, S. Giri, Stability, Reactivity, and Aromaticity of Compounds of a Multivalent Superatom. J. Phys. Chem. A 111 (2007) 11116. (e) J. Padmanabhan, R. Parthasarathi, V. Subramanian, P. K. Chattaraj, Electrophilicity-Based Charge Transfer Descriptor. J. Phys. Chem. A 111 (2007) 1358.

[23] (a) R. C. Haddon, L. T. Scott, π-Orbital Conjugation and Rehybridization in Bridged Annulenes and Deformed Molecules in General: π-Orbital Axis Vector Analysis. Pure Appl. Chem. 58 (1986) 137. (b) R. C. Haddon, Chemistry of the fullerenes: The manifestation of strain in a class of continuous aromatic molecules. Science 261 (1993) 1545. (c) T. Lin, W.-D. Zhang, J. Huang, C. He, A DFT Study of the Amination of Fullerenes and Carbon Nanotubes: Reactivity and Curvature. J. Phys. Chem. B 109 (2005) 13755. (d) H. Prinzbach, A. Weller, P. Landenberger, F. Wahl, J. Worth, L. T. Scott, M. Gelmont, D. Olevano, B. Issendorff, Gas-Phase Production and Photoelectron Spectroscopy of the Smallest Fullerene, C_{20}. Nature 407 (2000) 60. (e) Z. Chen, T. Heine, H. Jiao, A. Hirsch, W. Thiel, P. v. R. Schleyer, Theoretical Studies on the Smallest Fullerene: From Monomer to Oligomers and Solid States. Chem. Eur. J. 10 (2004) 963. (f) A. Hirsch, Z. Chen, H. Jiao, Spherical Aromaticity in I_h Symmetrical Fullerenes: The $2(N+1)^2$ Rule. Angew. Chem. Int. Ed. 39 (2000) 3915–3917. (g) M. N. Huda, A. K. Ray, Evolution of SiC nanocluster from carbon fullerene, a density functional theoretic study. Chem. Phys. Lett. 457 (2008) 124. (h) R. W. Alder, M. E. Blake, J. M. Oliva, Diaminocarbenes; Calculation of Barriers to Rotation about $C_{carbene}$-N Bonds, Barriers to Dimerization, Proton Affinities and ^{13}C NMR Shifts. J. Phys. Chem. A 103 (1999) 11200.

[24] R. Hoffmann, P. v. R. Schleyer, H. F. Schaefer, Predicting Molecules—More Realism, Please!. Angew. Chem. Int. Ed. 47 (2008) 7164.